1   **Title: The structural basis of the enhanced pollutant-degrading capabilities of an engineered**

2   **biphenyl dioxygenase**

3   **Running Title: Structural Studies of BphAE variant II9**

4   Sonali Dhindwal[1], Leticia Gomez-Gil[2], David B. Neau[3], Thi Thanh My Pham[4], Michel Sylvestre[4],

5   Lindsay D. Eltis[2], Jeffrey.T. Bolin[5], Pravindra Kumar[1][†]

6   [1]Department of Biotechnology, Indian Institute of Technology Roorkee, Roorkee, Uttarakhand 247667,

7   India

8   [2] Departments of Microbiology and Biochemistry, Life Sciences Institute, The University of British

9   Columbia, Vancouver, BC V6T 1Z3, Canada

10 [3]Department of Chemistry and Chemical Biology, Cornell University, Northeastern Collaborative

11 Access Team, Argonne National Laboratory, Argonne, Illinois 60439

12 [4]Institut National de Recherche Scientifique (INRS-Institut Armand-Frappier), Laval, Québec H7V

13 1B7, Canada

14 [5]Department of Biological Sciences and Center for Cancer Research, Purdue University, West

15 Lafayette, IN 47907, USA

16 [†] Corresponding Author

17 **Keywords:** biphenyl dioxygenase, BphAE, family shuffling, bioremediation, PCB

18 **Abbreviations used:** DDT- dichlorodiphenyltrichloroethane; BPDO- biphenyl dioxygenase; PCB-

19 polychlorinated biphenyl, bph- biphenyl

20   **Abstract**

21   Biphenyl dioxygenase, the first enzyme of the biphenyl catabolic pathway, is a major determinant of

22   which PCB congeners are metabolized by a given bacterial strain. Ongoing efforts aim to engineer

23   BphAE, the oxygenase component of the enzyme, to efficiently transform a wider range of congeners.

24    $BphAE_{II9}$, a variant of $BphAE_{LB400}$ in which a seven-residue segment, [335]TFNNIRI[341], has been

25   replaced by the corresponding segment of $BphAE_{B356}$, [333]GINTIRT[339], transforms a broader range of

26   PCB congeners than either $BphAE_{LB400}$ or $BphAE_{B356}$, including 2,6-dichlorobiphenyl, 3,3'-

27   dichlorobiphenyl, 4,4'-dichlorobiphenyl, and 2,3,4'-trichlorobiphenyl. To understand the structural

28   basis of the enhanced activity of $BphAE_{II9}$, we have determined the three-dimensional structure of this

29   variant in substrate-free and biphenyl-bound forms. Structural comparison with $BphAE_{LB400}$ reveals a

30   flexible active site mouth and a relaxed substrate binding pocket in $BphAE_{II9}$ that allow it to bind

31   different congeners, and which could be responsible for the enzyme's altered specificity. Biochemical

32   experiments   revealed   that $BphAE_{II9}$ transformed   2,3,4'-trichlorobiphenyl   and   2,2',5,5'-

33   tetrachlorobiphenyl more efficiently than $BphAE_{LB400}$ and $BphAE_{B356}$ did. $BphAE_{II9}$ also transformed

34   the insecticide DDT more efficiently than either parental enzyme (apparent $k_{cat}/K_m = 2.2 \pm 0.5$ $vs.$ $0.9 \pm$

35   0.5 $mM^{-1}s^{-1}$ for $BphAE_{B356}$). Docking studies of the enzymes with these three substrates provide insight

36   into the structural basis of the different substrate selectivity and regiospecificity of the enzymes.

37   **Importance**

38   Biphenyl dioxygenase is the first enzyme of the biphenyl degradation pathway that is involved in

39   degradation of polychlorinated-biphenyls. Attempts have been made to identify the residues that

40   influence the enzyme activity for the range of substrates among various species. In this study we have

41   done the structural study of one variant of this enzyme that was produced by family shuffling of genes

42   from two different species.   Comparing the structure of this variant with the parent enzymes has

43 provided an important insight towards the molecular basis for the broader substrate preference of this

44 enzyme. The structural and functional details gained in this study can be utilized to further engineer

45 desired enzymatic activity, producing more potent enzymes.

46 **Introduction**

47 The microbial degradation of environmental pollutants has been extensively studied over the past few

48 decades (1-3). Some pollutants, including polychlorinated biphenyls (PCBs), pose a threat to human

49 health and to the biosphere due to their toxicity and persistence. Apprehension about PCBs led to

50 prohibition of their production and use as well as regulation of their disposal and/or remediation (3-7).

51 Bacterial degradation plays a pivotal role in bioremediation of PCB-contaminated soil and water (8-

52 10). Aerobic degradation involves the biphenyl (Bph) catabolic pathway, which includes four enzyme-

53 catalyzed reactions. Bacteria can utilize the Bph pathway to co-metabolize a variety of PCB congeners

54 with differential effectiveness and different PCB congeners are transformed in a strain-dependent

55 fashion (11). Till now, structural studies have been done for all four enzymes to understand the detailed

56 mechanism that underlies this pathway (12-17).

57 Biphenyl dioxygenase (BPDO), the first enzyme of the Bph pathway, is a three-component ring-

58 hydroxylating Rieske-type oxygenase (RO) that utilizes NADH and O_2 to transform biphenyl to *cis-*

59 (*2R,3S*)-dihydro-dihydroxybiphenyl, Fig 1(A). The three components are a two-subunit oxygenase

60 (BphAE), a ferredoxin (BphF), and a ferredoxin reductase (BphG) (18, 19). BphF and BphG deliver

61 electrons from NADH to the oxygenase. As is typical of ring-hydroxylating ROs, the oxygenase is a

62 three-fold symmetric heterohexamer assembled from three larger BphA (α) subunits and three smaller

63 BphE (β) subunits such that the overall shape resembles that of a mushroom with the three α subunits

64 forming the cap and the three β subunits forming the stem. Each α-subunit includes a [2Fe-2S] Rieske-

65   type cluster (His_2Cys_2 ligation) involved in electron transfer from external reductants to an active site

66   containing a mononuclear Fe^{2+} ion coordinated by two His residues, an Asp residue (His233, His239,

67   and Asp388 in $BphAE_{LB400}$ (12)), and a conserved water molecule. The 3-fold symmetric arrangement

68   of αβ dimers brings the [2Fe-2S] cluster of one dimer close to the active site of another, such that the

69   Rieske center of one α-subunit is 12 Å from the Fe^{2+} atom of the neighboring subunit. It is generally

70   accepted that electron transfer from the Rieske cluster to the Fe^{2+} occurs through a network of

71   hydrogen bonds and Asp230 plays a major role in connecting the sites (20, 21).

72   The enzymatic capabilities of BPDO have been studied extensively because its substrate preference and

73   the nature of the reaction products are major determinants of the transformations of different PCBs by

74   the Bph pathway. For the purpose of bioremediation, it is desirable to expand the range of PCB

75   congeners transformed by the Bph pathway. Accordingly, an extensive effort in enzyme engineering

76   has been directed toward broadening the substrate range of BPDO. For example, relatively unbiased

77   directed evolution has been used to alter the substrate profiles of variants derived from the closely

78   related BPDOs of *Burkholderia xenovorans* LB400 and *Pseudomonas pseudoalcaligenes* KF707, two

79   bacterial strains that degrade PCBs relatively well (22, 23). An alternative, more targeted strategy took

80   into account comparisons of amino acid sequences and functional properties by Mondello *et al.*, which

81   identified four regions (I-IV) in the C-terminal domain of BphA that modulate the regioselectivity and

82   regiospecificity of the enzyme (24). By shuffling the segment of *bphA* encoding the C-terminal portion

83   of the *B. xenovorans* LB400 and *Pandoraea pnomenusa* B356 enzymes, Barriault *et al*. obtained

84   several variants that exhibited an expanded substrate range (25).

85   Several of the most potent PCB-transforming BphAE variants have been derived from $BphAE_{LB400}$

86   (26-28). $BphAE_{II9}$ is a variant of $BphAE_{LB400}$ in which the seven residues of Region

87   III, ^{335}TFNNIRI^{341}, are replaced by the corresponding residues of $BphAE_{B356}$, ^{333}GINTIRT^{339}. Among

88   other characteristics, BphAE$_{II9}$ is able to transform 2,3,4'-trichlorobiphenyl more efficiently than either

89   parental enzyme (29). BphAE$_{II10}$ adds a single residue substitution to the BphAE$_{II9}$ background:

90   Ala267 is replaced by Ser as occurs in BphAE$_{B356}$. Interestingly, the substrate range of BphAE$_{II10}$ is

91   significantly narrower than that of BphAE$_{II9}$. Finally, BphAE$_{P4}$ was created by substituting two

92   residues in Region III of BphAE$_{LB400}$: T335A and F336M (26). In liquid culture depletion assays, this

93   variant eliminates several congeners better than BphAE$_{LB400}$ does, including the very persistent 2,6-

94   dichlorobiphenyl (26). Structural analysis revealed that the altered substrate specificity of BphAE$_{P4}$ is

95   associated both with changes in direct side chain-substrate interactions and with changes in residue-

96   residue interactions near the active site; the latter appear to relieve constraints on the induced fit

97   between the enzyme and substrates (12).

98   In the current study, we analyzed the crystal structure of BphAE$_{II9}$ in the absence and presence of

99   biphenyl to elucidate the molecular basis for the broader substrate preference of the enzyme. We

100 focused on Region III residues to better understand how their interactions with other residues modulate

101 substrate competence and reaction regiospecificity. Further, we report the results of biochemical assays

102 and docking experiments with selected chlorinated biphenyl analogs and the insecticide 1,1,1-trichloro-

103 2,2-*bis*(4-chlorophenyl)ethane (also known as dichlorodiphenyltrichloroethane, DDT) directed toward

104 identification of the structural features in BphAE$_{II9}$, BphAE$_{LB400}$, and BphAE$_{B356}$ responsible for the

105 differential ability of the enzymes to transform these compounds.

106 **Experimental Procedures**

107 *Manipulation of DNA and preparation of BphAE$_{II9}$ protein*

108 The DNA for BphAE$_{II9}$, a variant of BphAE$_{LB400}$, was obtained in a previous study by shuffling

109 targeted regions of the *bphA*$_{LB400}$ and *bphA*$_{B356}$ genes (25). Gene *bphAE*$_{II9}$ DNA was cloned in pET14b

110   and transformed into *Escherichia coli* C41(DE3). BphAE$_{II9}$ was produced in that strain as a His-tagged

111   recombinant protein and purified by affinity chromatography according to protocols published for

112   BphAE$_{LB400}$ (27).

Crystallographic Procedures

114   Crystallization experiments were performed at 21°C in a glove box (Innovative Technologies,

115   Newburyport, MA) with a circulating N$_2$ atmosphere (<5 ppm oxygen). Good quality, diffracting

116   crystals were obtained from BphAE$_{II9}$ by sitting drop vapor diffusion using a well solution of 20 – 25%

117   PEG 8000, 6% glycerol, 50 mM NaCl, and 50 mM 2-(N-morpholino)ethanesulfonic acid (MES), pH

118   6.0. Crystals of the biphenyl-bound form of BphAE$_{II9}$ were obtained by adding a small amount of

119   powdered biphenyl (purchased from Sigma-Aldrich http://www.sigmaaldrich.com) directly to

120   crystallization drops containing BphAE$_{II9}$ crystals and incubating for 30 minutes before harvesting the

121   crystals. Diffraction data from crystals flash frozen by immersion in liquid N$_2$ were collected at the

122   BioCARS 14BM-C beamline at the Advanced Photon Source (Argonne National Laboratories). Data

123   were acquired for both substrate-free and biphenyl-bound crystals. The diffraction data were indexed,

124   integrated, and scaled using the HKL2000 program suite.

125   Initial phases were obtained by molecular replacement using MOLREP from the CCP4 v.6.3.0 software

126   suite (30, 31). The crystal structure of a single αβ heterodimer of BphAE$_{LB400}$ (PDB ID: 2XRX) was

127   used as a search model. REFMAC 5.2 (32) was used for rigid body refinement of the molecular

128   replacement model and for subsequent rounds of restrained atomic parameter refinement. The program

129   COOT was used for analysis of electron density maps and model building (33). Solvent molecules, Fe

130   ions (for the Rieske clusters and mononuclear Fe^{+2}), and biphenyl molecules were added where the F_o -

131   F_c map had features of appropriate volume above 3σ and the 2F_o - 2F_c map showed density at 1σ. The

132   stereochemical properties of the refined models were evaluated using the program MOLPROBITY

133   (34). The data collection, refinement statistics, and model quality for the two structures are summarized

134   in Table 1. All molecular figures were prepared using the program PyMOL (35).

135   ***Assays and kinetic studies of BPDO from wild type and variant***

136   DDT (99% pure) was obtained from Sigma-Aldrich, 2,3,4'-trichlorobiphenyl and 2,2',5,5'-

137   tetrachlorobiphenyl were obtained from Ultra Scientific. The ability of $BphAE_{LB400}$, $BphAE_{B356}$, and

138    $BphAE_{II9}$ to metabolize 2,3,4'-trichlorobiphenyl and 2,2',5,5'-tetrachlorobiphenyl and DDT was

139   assessed using BPDO systems reconstituted from His-tagged components produced and purified as

140   described previously (12). The enzyme assays were performed in 200 μl of solution containing 100 to

141   800 nmol substrate and buffered with 50 mM MES, pH 6.0 at $37^{o}C$ as described previously (36).

142   Metabolites were identified by GC-MS analysis after the reaction medium was incubated for 15 min.

143   The metabolites were extracted at pH 6.0 with ethyl acetate, then treated with *n*-butylboronate (*n*BuB)

144   prior to GC-MS analysis, as described previously (37) using a Hewlett Packard HP6980 series gas

145   chromatograph interfaced with an HP5973 mass selective detector (Agilent Technologies). To obtain

146   kinetic parameters with DDT as substrate, metabolite production was monitored by HPLC and UV/Vis

147   spectrometry according to a protocol described previously (38).

148   ***Docking Studies***

149   Molecular docking of substrates was accomplished using the Schrödinger, Maestro^{TM} suite; version-9.1

150   (Glide^{TM}, version 2.6, Schrodinger, Inc., New York) (39). The crystal structures of $BphAE_{LB400}$ (PDB

151   ID: 2XRX), $BphAE_{II9}$, and $BphAE_{B356}$ (PDB ID: 3GZX) with bound biphenyl were prepared for

152   docking using Maestro's protein preparation wizard: hydrogens were added, bond orders were

153   assigned, and the structure was energy minimized using the OPLS2001 force-field until the rmsd

154   between the minimized structure and the starting structure reached 0.3Å. For each of the prepared

155   protein structures, a 12x12x12 Å receptor grid box was erected using the centroid of the atoms in the

156   bound biphenyl as the center of the box. The substrates, DDT, 2,3,4'-trichlorobiphenyl and 2,2',5,5'-

157   tetrachlorobiphenyl, were prepared using Maestro's Ligprep module (Ligprep, Schrodinger, Inc., New

158   York, NY). Glide^{TM} was then used for docking of the substrates using the Extra Precision (XP) mode

159   (40, 41). The best conformation was selected on the basis of the Glide score and Emodel value. Visual

160   inspection was used to confirm that the substrates were docked in a plausible orientation similar to that

161   observed in the crystal structure of the BphAE$_{LB400}$:biphenyl complex.

162   **Results and Discussion**

163   *Crystal structures of BphAE$_{II9}$ substrate-free and biphenyl-bound forms*

164   The crystal structures of the substrate-free and biphenyl-bound forms of BphAE$_{II9}$ were determined to

165   resolutions of 2.5 Å and 1.9 Å, respectively. Representative crystallographic data and refinement

166   statistics are presented in Table 1.

167   Coordinates and structure factors for both structures were deposited in the Protein Data Bank with the

168   identifiers 5AEU (substrate-free) and 5AEW (biphenyl bound).

169   The crystal structure of the substrate-free form was refined at a resolution of 2.5 Å to final R_{cryst} and

170   R_{free} values of 18.1% and 23.4%, respectively, with four αβ heterodimers in the asymmetric unit of

171   space group H3. Three dimers form one biological hexamer ($α_3β_3$) associated with the asymmetric

172   unit, and the fourth forms a hexamer with symmetry related heterodimers. The final model includes

173   residues 18 to 143 and 153 to 459 for all α-subunits and residues 6 to 188 for all β-subunits.

174   Interpretable electron density was not observed for residues 144 to 152 of the α-subunit. These residues

175 were also absent in the wild type BphAE$_{LB400}$ structure (12). Similar to other Rieske-type

176 dioxygenases, each α-subunit binds a [2Fe-2S] Rieske-type cluster and a mononuclear Fe^{2+} ion at the

177 active site, which is coordinated to two His residues (His233 and His239), an Asp residue (Asp388),

178 and one or more water molecules.

179 The biphenyl bound structure was refined to a final R_{cryst} of 21.6% and R_{free} of 25.4%, respectively, at a

180 resolution of 1.9 Å in space group P1. The structure includes twelve crystallographically independent

181 αβ heterodimers. α-subunits are labeled chains A, C, E, G, etc., and β subunits are chains B, D, F, H,

182 etc. The final model includes residues 18 to 143 and 153 to 459 for all α-subunits except chain U

183 (missing residues 143 and 459) and chain W (missing residue 143). For the β-subunits, all chains

184 extend to residue 188, but the N-terminal content varies among the chains: chain F begins at residue 5,

185 chain J begins at residue 14, and the remaining chains begin within the range of residues 6 to 13.

186 In eight of the α-subunits (C, E, I, K, M, O, Q, and W), initial unbiased (Fo-Fc) Fourier maps showed

187 bulky electron density at the active site consistent with bound biphenyl, Fig 1(B), whereas such density

188 was not observed for the other four α-subunits (chains A, G, S, and U). Density consistent with a

189 partially occupied biphenyl was observed for chain S at a later stage.

190 Absence of biphenyl in some active sites appears to be a consequence of crystal packing contacts

191 associated with structural variation in the N-terminal segments of the β subunits. For most β subunits,

192 the N-terminal segment interacts with residues of the same subunit or an adjacent β subunit of the same

193 α$_3$β$_3$ hexamer. But for three β subunits (D, F, and J), the N-terminal segment extends away from the

194 rest of the β subunit and interacts with a loop formed by α-subunit residues 247-263 at the mouth of

195 one of the actives site of a neighboring α$_3$β$_3$ hexamer. This contact apparently interferes with binding

196 of biphenyl. In fact, for chains D and F, the side chain of β-Phe9 extends just into the mouth of the

197   active site of a neighboring α-subunit (chains A and G, respectively) and would prevent entry of

198   substrate into the active site, as shown in Supplementary Fig 1. In the case of chain J, β-Phe9 was not

199   modeled because interpretable electron density begins at residue 14. Nevertheless, the N-terminal

200   segment in chain J extends towards chain U and density for biphenyl was not observed in the active site

201   of U.

202   *Interactions, conformation, and orientation of biphenyl*

203   As observed in prior structures of biphenyl dioxygenases, the substrate binding pocket of $BphAE_{II9}$ is

204   sandwiched between the core *β*-strands and α-helices of the α-subunit. Biphenyl binds at the active site

205   in a non-planar conformation with the ring closer to the Fe^{2+} surrounded by residues Gln226, Phe227,

206   Asp230, Met231, His233, and His323. The distal ring is surrounded by Ala234, His239, Ser283,

207   Val287, Gly321, Gln322, Leu333, Ile336, Phe378, and Phe384, Fig 1(B). Non-planarity manifests

208   through torsion about the C1-C1P bond, which averages -52° and ranges from -37° to -67°.

209   Consistent with a 2,3-dioxygenation of the substrate, the C2 and C3 atoms of biphenyl are generally

210   closer to the Fe^{2+} ion than is C1: the average distances are 4.5 Å for C2 and C3, and 5.1 Å for C1.

211   Despite variations in the C2-Fe^{2+} and C3-Fe^{2+} distances in the range 4.2 Å to 4.8 Å, in no case is either

212   C2 or C3 significantly closer to Fe^{2+}. Further, superposition of the α-subunits on the basis of Cα atoms

213   (as described below) places the proximal rings in a tight cluster, as shown in Fig 2(B). The same

214   superposition shows greater variability in the relative positions of the distal rings. This variance in the

215   position of the distal ring is also seen in the structure of biphenyl bound $BphAE_{LB400}$. However, the

216   proximal ring binds in a similar fashion with respect to the Fe^{2+} ion in all chains.

217   Water molecules in contact with biphenyl and bound to Fe^{2+} were modeled in three different locations

218   among the several active sites, and either one or two waters were included. Two of the locations

219 correspond to the site of side-on binding of dioxygen observed in crystal structures of naphthalene

220 dioxygenase (42), whereas the third site lies on the opposite side of a plane defined by C2, C3, and

221 Fe^{2+}. Based on the quality of the active site density and the reliability of the atomic coordinates (judged

222 by B factors), the active site models for chains C and O are the most reliable.

223 ***Comparison among α-subunits of the substrate-free and biphenyl-bound structures of BphAE$_{II9}$***

224 The Cα atoms of the α-subunits from the substrate-free and biphenyl-bound BphAE$_{II9}$ structures, 16

225 chains in total, can be superposed with a Cα rmsd of 0.5 Å or less, demonstrating close agreement. In

226 some regions, however, variations in the local structure are observed.

227 Examination of superposed αβ dimers reveals that the BphAE$_{II9}$:biphenyl complex shows greater

228 variability in the position of key active site elements as shown in Fig 2(B) than either the substrate-free

229 BphAE$_{II9}$ structure, Fig 2(C), or the biphenyl-bound form of its progenitor, BphAE$_{LB400}$, Fig 2(A). For

230 example, in the latter two crystal structures, the superposed positions of the Fe^{2+} ions lie in single, tight

231 clusters. By contrast, in the BphAE$_{II9}$:biphenyl complex, five Fe^{2+} ions (chains A, C, E, G, and U) are

232 in one cluster and six (I, K, M, O, Q, and W) are found in a second cluster ~1.3 Å distant (average of

233 all intercluster Fe^{2+}- Fe^{2+} distances). Although the first cluster includes all chains for which biphenyl is

234 not modeled (A, G, and U), two active sites with biphenyl present (C, E) are also members. The Fe^{2+}

235 from chain S lies approximately between the two clusters and nearly equidistant (0.8 Å) from both.

236 Comparatively greater positional variability is also observed in the BphAE$_{II9}$:biphenyl complex for two

237 of the Fe^{2+} coordinating residues, Asp388 and His239, as well as Ser283, Val287, Gly321, and Gln322.

238 The case of Asp388 is highlighted in Fig 2(A, B, and C). Although the carboxylate groups of Asp338

239 for all chains lie close to a common plane, the Cδ atoms are as much as 1.5 Å apart. The variations for

240 Asp388 extend to the backbone atoms: the average (0.8 Å) and maximum (1.5 Å) distances among Cα

241   atoms are indistinguishable from the average and maximum for $C\gamma$ and $O\delta1$, which binds to the Fe^{2+}.

242   Ligands would be expected to track with the Fe^{2+}, and thus clusters are again observed for the Asp388

243   carboxylates, although they are not as distinct or as tightly clustered.

244   To understand the variations in Fe^{2+} and Asp388 locations it is useful to consider them with reference

245   to a vector from the $C\alpha$ atom of Gly321 to the $C\alpha$ of Asp388, which passes close to the center of

246   biphenyl and close to the Fe^{2+}. The length of the vector is significantly shorter for chains without

247   density for biphenyl, ($\acute{r} = 15.0$ Å, range $=$ 15.0 Å to 15.1 Å) compared to chains with biphenyl

248   ($\acute{r} = 16.5$ Å, range $=$ 15.9 Å to 17.3 Å). Qualitatively, expansion of the active site along this vector

249   moves the Fe^{2+} and Asp388 away from Gly321 opening space for biphenyl.

250   The orientation of the peptide plane between Gly321 and Gln322 and the interactions of the carbonyl of

251   Gly321 also differ between the substrate-free and biphenyl complex and vary among the chains of the

252   latter, Fig 3(A). In all four chains of the $BphAE_{II9}$ substrate-free structure, ψ is in the range 12° to 37°

253   such that the carbonyl of Gly321 is points into the active site and interacts with $C\varepsilon$ of Met231 through a

254   distance of 3.0 Å to 3.2 Å. For the biphenyl soaked structure, the carbonyl of Gly321 is similarly

255   placed in six of the chains including all three without density for biphenyl (A, G, and U) and three with

256   biphenyl modeled (M, Q, and W). In the other six chains, all with biphenyl modeled (C, E, I, K, O, and

257   S), ψ is in the range 95° to 115°, such that the direction of the carbonyl of Gly321 differs by ~90°.

258   This allows the carbonyl to form a hydrogen bond with the amide NH of Tyr277 through a distance of

259   3.0 Å to 3.1 Å. As in the case of the Fe^{2+} location, the local structures of chains without biphenyl

260   modeled are consistent, but the chains with biphenyl bound disperse between two groups, one that is

261   consistent with the substrate-free structure and one that is distinct.

262 A difference in extent of variability between the biphenyl complex and the substrate-free enzyme is

263 also seen for the short α-helix (Pro281-Met288) that forms one side of the active site portal and one

264 wall of the biphenyl binding site, where the side chains of Ser283 and Val287 are in contact with the

265 distal ring of biphenyl. In the BphAE$_{II9}$ biphenyl complex, the maximum difference in the positions of

266 Ser283 Cα atoms for any pair of chains is 1.9 Å, but among the chains in the BphAE$_{II9}$ substrate-free

267 structure the maximum value of the same measure is 0.6 Å.

268 Finally, a comparable extent of variability is seen in both structures for the backbone and side chain

269 atoms from residue Pro249 to Thr260. Here, the maximum Cα displacement of upto 0.8 Å & 2 Å in

270 BphAE$_{II9}$ biphenyl bound structure and upto 3.8 Å & 1.1 Å is seen in BphAE$_{II9}$ biphenyl free structure

271 at residues Ser254 & Ile258 respectively. A comparable variation is observed for side chain atom

272 positions and conformations. This segment contains a large fraction of solvent exposed residues and

273 does not contribute directly to the biphenyl binding.

274

275 ***Observed structural changes due to shuffled Region III***

276 Previous studies suggested that each residue in Region III can influence the functional properties of the

277 enzyme by direct or indirect interactions with active site residues (12, 27). We have compared the

278 structure of BphAE$_{II9}$ with those of the parental enzymes, BphAE$_{LB400}$ and BphAE$_{B356}$, to consider the

279 influence of specific substitutions on the oxygenase's functional properties. BphAE$_{II9}$ has four

280 substitutions in Region III with respect to BphAE$_{LB400}$: Thr335Gly, Phe336Ile, Asn338Thr, and

281 Ile341Thr. In a previous report (29), we showed that the k_{cat} value of BphAE$_{II9}$ and BphAE$_{LB400}$

282 toward biphenyl is similar. This indicates that the structural changes brought by these substitutions did

283   not alter the electron transfer system in BphAE$_{II9}$. However, as we will see below, the structural

284   analysis shows each of these substitutions may contribute to increase flexibility of the active site.

285   <u>The Thr335Gly substitution</u>: In BphAE$_{LB400}$, a hydrogen bond between Thr335 Oγ and Gly321 N

286   presumably restricts the conformation of the Val320-Gly321 dipeptide. The Thr335Gly substitution in

287   BphAE$_{II9}$ abolishes the hydrogen bond, and the Val320-Gly321 segment, which lines the active site

288   pocket, is more relaxed, Fig 3(B). As noted above, the 321-322 peptide plane exists in two orientations

289   among the chains of the biphenyl complex. One of these, as illustrated by chain C, would accommodate

290   bulkier substrates. For example, for chain C of BphAE$_{II9}$:biphenyl complex, a ψ angle of 107° at

291   Gly321 increases the distance between the carbonyl oxygen of Gly321 and *ortho* and *meta* carbon

292   atoms of biphenyl's distal ring to 5.4 Å and 5.0 Å, respectively. These distances are typically 4 Å or

293   less in the BphAE$_{LB400}$:biphenyl complex.

294   As was the case for the previously studied BphAE$_{LB400}$ variant BphAE$_{p4}$, the substitution of Thr335 by

295   a smaller amino acid such as Ala in BphAE$_{p4}$ or Gly in BphAE$_{II9}$ eliminates a hydrogen bond between

296   the Thr335 Oγ and Gly321 N, relieving a conformational constraint on the Val320-Gly321 dipeptide,

297   residues that line the active site of the protein (12). Due to the absence of this constraint on Gly321, the

298   carbonyl of the peptide bond between Gly321 and Gln322, which points towards the active site in

299   BphAE$_{II9}$ substrate-free structure, points away from the substrate binding site in BphAE$_{II9}$-biphenyl

300   bound structure. This makes more space in the active site for the binding of bulkier substrates. Also, in

301   the presence of biphenyl, Val320 in BphAE$_{II9}$ is displaced from its original position by 1.0 Å and

302   makes polar contact with Ser283. At its new position, Ser283 interacts with the main chain of residues

303   Ala286 and Val287. This is responsible for the variability in the position of the short α-helix (Pro281-

304   Met288).

305   The Phe336Ile substitution: The Phe336Ile substitution places a smaller side chain at the surface of the

306   active site, directly increasing the volume available for substrate binding. The minimum distance

307   between residue 336 and *meta* and/or *para* carbons of biphenyl's distal ring increases from 3.6 Å

308   (median) for $BphAE_{LB400}$ ($Phe336_{LB400}$ Cε and/or Cζ in a -60,-40 rotamer) to 4.1 Å (median) for

309     $BphAE_{II9}$ ($Ile366_{II9}$ Cδ1 in a -60,-60 rotamer). Moreover, the minimum distance increases to 5.1 Å in

310   chain Q wherein $Ile366_{II9}$ assumes a readily accessible -60,-60 rotamer. It should be noted that

311   mutation to Ile336 affects the conformation of a neighboring residue, Phe378, pushing it closer to

312   biphenyl, Fig 3(C), such that $Phe378_{II9}$ Cζ approaches the *ortho* and/or *meta* atoms of the distal ring.

313   The typical closest contact distances remain longer than 4 Å, but distances as short as 3.7 Å were

314   observed. These contact distances can be readily altered by a change in the torsion angle between

315   biphenyl's rings, whereas contacts between the side chain of residue 336 and the *para* carbon are

316   unaffected by the conformation of biphenyl.

317   The Asn338Thr substitution: In this case, an effect mediated by the difference in chain length of Thr

318   and Asn are conceivable. For both variants, the side chain oxygen atom accepts a hydrogen bond from

319   the Nε of neighboring residue, Arg340. It is clearly seen that due to the difference in side chain length

320   of Asn and Thr, the side chain of Arg340 is placed at different positions in $BphAE_{LB400}$ and $BphAE_{II9}$,

321   respectively, Fig 3(D). While, a hydrogen bond between Arg340 Nη2 and the carbonyl of Phe378 is

322   clearly visible in $BphAE_{LB400}$ structure, it is not observed in $BphAE_{II9}$. This impedes the movement of

323   the side chain of Phe378 in $BphAE_{LB400}$ but not in $BphAE_{II9}$. As mentioned above, Ph378 lies close to

324   the active site and the freedom associated with its side chain can easily affect the orientation of the

325   bound substrate. In $BphAE_{II9}$, the phenyl ring of Phe378 is 4.9 Å away from the vicinal ring and 4.4 Å

326   away from the distal ring of the biphenyl. These distances in $BphAE_{LB400}$ are 5.5 Å from the vicinal

327   and 4.9 Å from the distal ring of the substrate. Thus, the type of residue at position 338 indirectly

328   affects the orientation and the position of oxygenation of substrate at the active site.

329   The Ile341Thr substitution: The influence of this substitution on substrate range or other aspects of

330   enzyme activity remains enigmatic from the perspective of the crystal structures. Relative to the

331   biphenyl binding site, the side chain for position 341 lies on the opposite surface of the central β sheet

332   and its Cβ atom is more than 14 Å distant from the closest atom of biphenyl. Significant changes in

333   local backbone conformation are not observed, and minor changes in the placement or conformation of

334   neighboring side chains directed toward the active site (Arg340 and Trp342) cannot be attributed

335   uniquely to the Ile341Thr substitution.

336   Therefore, except for the Ile341Thr substitution, structural analysis clearly shows the other three

337   substitutions in $BphAE_{II9}$ may contribute to the expanded substrate range of the enzyme. The indirect

338   effect of Phe336Ile, Asn338Thr, and Ile341Thr substitutions on the active site influences the

339   constraints placed on Phe378, a residue that lines the active site and is particularly close to the bound

340   biphenyl, Fig 4. The Asn338Thr and Ile341Thr substitutions appear to act together pulling the Arg340

341   side chain away from the backbone carbonyl of Phe378. As a consequence the hydrogen bond

342   involving Arg340 and Phe378 of $BphAE_{LB400}$ is eliminated in $BphAE_{II9}$ freeing at least one major

343   constraint on the position of Phe378. In contrast the Phe336Ile substitution acts more directly on the

344   position of Phe378, by displacing the ring of Phe378 in the direction of the Fe^{2+}. Interestingly, by

345   comparing the position of $Phe378_{LB400}$ to the corresponding $Phe376_{B356}$, $Phe376_{B356}$ exhibits a shift

346   towards the Fe^{2+} as well, Fig. 4.

347   Thus, although the chains modeled in the structures of $BphAE_{II9}$ substrate-free and biphenyl-bound

348   forms show a high degree of similarity with each other and with the chains of $BphAE_{LB400}$, there are a

349   number of conformational variations within localized regions. The regions of high variability

350   (specifically the iron ligands Asp388 and His239, the residues Gly321 and Gln322, the α-helix Pro281-

351   His288, and the region of Pro249 through Thr260) demonstrate a high degree of flexibility in and

352   around the active site, Fig 4.   Some of this flexibility, for example the Pro249-Thr260 region, is

353   observed in the parent enzyme, but much of it appears unique to BphAE$_{II9}$.

354   Additionally, variation was seen in the binding position and orientation of biphenyl in various αβ-

355   heterodimers of the BphAE$_{II9}$ biphenyl-bound structure. First, the variation in distance from the Fe^{2+} to

356   the vicinal ring of biphenyl demonstrates a structure with a high tolerance for a variety of substrate

357   binding. Next, the variation seen in the position of the distal ring of biphenyl demonstrates a binding

358   pocket that has a volume larger than is necessary to bind biphenyl, and is capable of binding larger

359   substrates. These aspects of substrate binding again point to a relaxed active site capable of

360   accommodating a variety of substrate analogs which explains the ability of BphAE$_{II9}$ to metabolize an

361   expanded range of PCB congeners.

362   Thus, although the chains modeled in the structures of BphAE$_{II9}$ substrate-free and biphenyl-bound

363   forms show a high degree of similarity with each other and with the chains of BphAE$_{LB400}$, there are a

364   number of conformational variations within localized regions. The regions of high variability

365   (specifically the iron ligands Asp388 and His239, the residues Gly321 and Gln322, the α-helix Pro281-

366   Met288, and the region of Pro249 through Thr260) demonstrate a high degree of flexibility in and

367   around the active site, Fig 4.   Some of this flexibility, for example the Pro249-Thr260 region, is

368   observed in the parent enzyme, but much of it appears unique to BphAE$_{II9}$.

369   **Transformation of 2,3,4'-trichlorobiphenyl, 2,2',5,5'-tetrachlorobiphenyl and DDT and Docking studies**

370   To provide more insight about the structural features in BphAE$_{II9}$, BphAE$_{LB400}$, and BphAE$_{B356}$

371   responsible for their differential ability to metabolize biphenyl analogs, we examined the biochemistry

372   and the structural interaction of these enzymes toward 2,2',5,5'-tetrachlorobiphenyl, 2,3,4'-

373   trichlorobiphenyl and DDT.

374   Biochemical studies were performed to assess the ability of BphAE$_{II9}$ to transform DDT and two PCB

375   congeners, 2,3,4'-trichlorobiphenyl, 2,2',5,5'-tetrachlorobiphenyl, and the regiospecificty of the

376   reactions.

377   BphAE$_{LB400}$ generated one major metabolite from 2,3,4'-trichlorobiphenyl as determined by

378   examination of the GC-MS profile of the assay solution, Fig 5(A). The mass spectral features of this

379   metabolite's nBuB derivative were consistent with those of a dihydro-dihydroxy-trichlorobiphenyl,

380   namely a fragmentation pattern exhibiting a molecular ion at m/z 356 and diagnostically important ions

381   at m/z 340 (M$^+$ - O), 321 (M$^+$ - Cl), 286 (M$^+$ - 2Cl), 256 (M$^+$ - nBuBO2). A second metabolite

382   exhibiting mass spectral features of a dihydro-dihydroxy-trichlorobiphenyl was also detected, but those

383   features are not observable in Fig 5(A) as this metabolite was only present in trace quantities. BphAE$_{II9}$

384   transformed 2,3,4'-trichlorobiphenyl into the same major metabolite as shown in Fig 5(A), however,

385   the amount produced was significantly greater. BphAE$_{B356}$ produced the same metabolite from 2,3,4'-

386   trichlorobiphenyl, and the amount produced was similar to BphAE$_{LB400}$ (not shown). Therefore, our

387   assay demonstrated that the major product produced by three enzymes is the same metabolite, and that

388   BphAE$_{II9}$ has a greater ability to degrade 2,3,4'-trichlorobiphenyl as demonstrated by the much larger

389   peak for the metabolite observed in the chromatogram. The substrate was docked into the active site of

390   the three enzymes.

391   For BphAE$_{LB400}$, 2,3,4'-trichlorobiphenyl docked with the C3 and C3-Chlorine atoms in approximately

392   the same location as the C2 and C4 atoms of biphenyl in its complex with BphAE$_{LB400}$, and the

393   proximal ring is in approximately the same plane as found in the biphenyl complex. This places the

394   dichlorinated ring in a location and orientation consistent with dioxygenation across the C4-C5 bond.

395   In this pose as shown in Supplementary Fig 2(B), C4 and C5 are 4.3 Å and 4.4 Å from the Fe^{2+} ion,

396   respectively, and 2.8 Å and 3.0 Å from a water molecule that occupies the presumed binding site for

397   dioxygen.

398   For $BphAE_{II9}$, docking of 2,3,4'-trichlorobiphenyl produced a pose consistent with the same regio- and

399   stereo-specificity as $BphAE_{LB400}$, but the binding mode is remarkably different, Fig 6(A and B) &

400   Supplementary Fig 2(B). The dichlorinated ring does not penetrate as deeply into the active site, such

401   that its location is comparable to that of the distal ring in the $BphAE_{II9}$:biphenyl complex. In addition,

402   relative to the biphenyl complex, the orientation of the dichlorinated ring is shifted by ~70°, and the

403   torsion angle between the rings is shifted by +110°. Nevertheless, the distances from C4 and C5 to the

404   water are 3.3 Å and 3.0 Å, and distances to the Fe^{2+} are 5.1 Å and 4.5 Å. For $BphAE_{B356}$, 2,3,4'-

405   trichlorobiphenyl docked in a manner similar to $BphAE_{II9}$ as shown in Supplementary Fig 2(A), but

406   with reduced docking scores.

407   Our docking study showed that the preferred docking pose for all three enzymes was one that

408   positioned the substrate to be converted to a 3,4-dihydro-3,4-dihydroxy-2,3,4'-trichlorbiphenyl. This

409   proposed product would not be further degraded into a chlorobenzoate, which may explain why in their

410   experiment with $BphAE_{LB400}$, Seeger *et al.* did not detect any chlorobenzoate produced from 2,3,4'-

411   trichlorobiphenyl since $BphAE_{LB400}$ metabolize this substrate through a 3,4-dioxygenation (43).

412   Further, the docking study showed that the preferred pose for $BphAE_{LB400}$ oriented the substrate much

413   further into the active site than the preferred pose for $BphAE_{II9}$, Fig 6(B) and Supplementary Fig 2(B).

414   This deeper binding mode may explain why $BphAE_{LB400}$ exhibits a lower activity towards 2,3,4'-

415   trichlorobiphenyl than $BphAE_{II9}$.

416   BphAE$_{II9}$ and BphAE$_{LB400}$ produced dihydro-dihydroxy-tetrachlorinated as the only metabolite of

417   2,2',5,5'-tetrachlorobiphenyl and on the basis of peak area, the amounts produced were approximately

418   the same for both enzymes, Fig 5(B). Consistent with a previous report (44), the dihydro-dihydroxy-

419   tetrachlorbiphenyl produced from 2,2',5,5'-tetrachlorobiphenyl by BphAE$_{II9}$ and BphAE$_{LB400}$ must

420   have been the 3,4-dihydro-3,4-dihydroxy-2,2',5,5'-tetrachlorobiphenyl and GC-MS analysis showed

421   that the metabolite produced by BphAE$_{II9}$ was the same as the one produced from BphAE$_{LB400}$.

422   The bulkier 2,2',5,5'-tetrachlorobiphenyl docked at the active sites of BphAE$_{LB400}$, BphAE$_{II9}$, and

423   BphAE$_{B356}$ in distinct locations and orientations, Fig 7(B). Once again, the deepest penetration was

424   found for BphAE$_{LB400}$, where docking of 2,2',5,5'-tetrachlorobiphenyl gave a single pose competent

425   for dioxygenation at C3 and C4, consistent with available biochemical data (Table 2). C3 and C4 are

426   almost equidistant from the key water molecule at 3.3 Å, and from the Fe^{2+} ion at 4.2 Å,

427   Supplementary Fig 3(B). The C5-chlorine faces towards His323, the C2-chlorine points towards

428   Phe384, and the proximal ring is nearly in the same as observed for the proximal ring of biphenyl in its

429   complex with BphAE$_{LB400}$.

430   In the active site of BphAE$_{II9}$, 2,2',5,5'-tetrachlorobiphenyl docked in multiple poses that would allow

431   *ortho-meta* dioxygenation across the C5-C6 or C2-C3 bonds as well as *meta-para* dioxygenation across

432   the C3-C4 bond. Since dechlorinated products were not observed in the biochemical analysis, poses

433   consistent with *ortho-meta* dioxygenation were ruled out for the purposes of this study. The orientation

434   most competent for *meta-para* dioxygenation, consistent with the biochemical data, was chosen for

435   further analysis although its docking metrics were lower. In this pose as shown in Fig 7(A), carbon 3

436   and 4 are 3.0 Å and 4.2 Å away from the water molecule and 4.1 Å and 5.4 Å away from the Fe^{2+} ion.

437   Unlike BphAE$_{LB400}$, the chlorine at the 2-C position of 2,2',5,5'-tetrachlorobiphenyl is positioned

438   towards His239 in BphAE$_{II9}$. The chlorine at the 5-C position faces toward His323 BphAE$_{II9}$, but in a

439   different orientation than in BphAE$_{LB400}$.

440   Interestingly, the docking experiments of the two enzymes showed very different preferred poses for

441   the binding of this substrate. The binding pose of 2,2',5,5'-tetrachlorobiphenyl in BphAE$_{II9}$ would

442   likely generate a steric conflict between the substrate and Phe336 if adopted in BphAE$_{LB400}$. The pose

443   adopted in BphAE$_{LB400}$, likewise, appears to be inaccessible to BphAE$_{II9}$, as it would create a steric

444   conflict with Phe378. But as discussed above Phe378 is less constrained in BphAE$_{II9}$ than in

445   BphAE$_{LB400}$. Therefore, Phe378$_{II9}$ may be more flexible in reality than was allowed in our docking

446   experiments which may explain the differences between the biochemical and the docking experiments.

447   For BphAE$_{B356}$, the best scoring pose places 2,2',5,5'-tetrachlorobiphenyl much further from the water

448   (4.1 Å and 4.3 Å) and Fe^{2+} (5.6 Å to both carbons) as compared to BphAE$_{LB400}$ and BphAE$_{II9}$,

449   Supplementary Fig 3(A) and Table 2. C3 and C4 are closest to the Fe^{2+}, but the increased distances

450   reflect a binding mode that is likely incompetent for the reaction, consistent with biochemical data that

451   show BphAE$_{B356}$ has poor activity towards 2,2',5,5'-tetrachlorobiphenyl.

452   BphAE$_{II9}$ retains activity towards 2,2',5,5'-tetrachlorobiphenyl while BphAE$_{B356}$ shows very little

453   activity towards that particular congener. This apparent contradiction is resolved when you consider the

454   role of an adjacent residue, Thr375$_{B356}$, on the position of Phe376$_{B356}$. Thr375$_{B356}$ Oγ1 makes a

455   hydrogen bond to the backbone carbonyl of Gln371$_{B356}$. This hydrogen bond forces Phe376$_{B356}$ to a

456   position closer to the Fe^{2+}, Fig 8. The corresponding residue to Thr375$_{B356}$ is Asn377$_{LB400/II9}$.

457   Asn377$_{LB400/II9}$ also forms hydrogen bond to the backbone carbonyl of His373$_{LB400/II9}$ (corresponding to

458   Gln371$_{B356}$) and with the backbone carbonyl of Val287$_{LB400/II9}$, Fig 8. This second interaction is

459   missing in BphAE$_{B356}$ and appears to anchor Phe378$_{II9}$ and restricts how far towards the Fe^{2+} the

460   residue can move, and thus seems responsible for preserving $BphAE_{II9}$'s activity towards 2,2',5,5'-

461   tetrachlorobiphenyl.

462   Based on this analysis one would expect that if $Thr375_{B356}$ was mutated to an Asn, $BphAE_{B356}$ could

463   potentially gain the ability to oxygenate 2,2',5,5'-tetrachlorobiphenyl. Indeed, $BphAE_{KF707}$, a strain

464   that exhibits no activity towards 2,2',5,5'-tetrachlorobiphenyl, gains the ability to oxygenate that

465   particular congener by a Thr376Asn substitution (corresponding to $Thr375_{B356}$ and $Asn377_{LB400/II9}$)

466   (45, 46). Likewise, the reverse is true, when $BphAE_{LB400}$'s Region III is replaced by Region III of

467   $BphAE_{KF707}$ along with mutating $Asn377_{LB400}$ to Thr (as in $BphAE_{KF707/B356}$) the enzyme loses its

468   activity against *ortho*-substituted congeners (47). However, it was also reported by Mondello *et al.* that

469   the $Asn377_{LB400}$Thr substitution alone (i.e. without swapping of Region III) did not affect the substrate

470   specificity of the mutated enzyme (24). Thus, neither the single Asn377Thr substitution, nor the

471   swapping of Region III alone appear to restructure $BphAE_{LB400}$ enough to disrupt its ability to act

472   against *ortho*-substituted congeners.

473   As reported previously (38), on the basis of product formation, the K_m and k_{cat} values of $BphAE_{B356}$

474   toward DDT were 174 ± 5 µM and 0.15 ± 0.08 s^{-1}, respectively. During the current work we found that

475   the activity of $BphAE_{LB400}$ towards DDT was too poor to calculate accurate steady-state kinetic values.

476   On the other hand, $BphAE_{II9}$ was able to metabolize DDT, exhibiting K_m and k_{cat} values of 82 ± 2 µM

477   and 0.18 ± 0.04 s^{-1}, respectively. The GC-MS chromatogram produced from $BphAE_{B356}$ against DDT

478   shows two metabolites identified as stereoisomers of 1,1,1-trichloro-2,(4-chlorophenyl-2,3-dihydroxy-

479   4,6-cyclohexadiene)-2-(4'-chlorophenyl)ethane as shown in Fig 5(C). $BphAE_{II9}$ produced the same two

480   stereoisomers but in inverse ratio to that of $BphAE_{B356}$, Fig 5(C).

481 The active sites of BphAE$_{II9}$, BphAE$_{LB400}$, and BphAE$_{B356}$ all accommodated DDT with corresponding

482 4-Cl-phenyl rings in similar locations. For the proximal ring, the distances between C4 atoms are 1.1 Å

483 - 1.4 Å, and the orientations of the rings are also similar, Fig 9 (B). Nevertheless, the placement of the

484 trichloromethyl group distinguishes the BphAE$_{LB400}$ complex from the others, and this complex had the

485 poorest docking metrics (Table 2).

486 For BphAE$_{II9}$, the top-ranked pose is consistent with dioxygenation across the C2-C3 bond, and the

487 trichloromethyl group is directed away from the Fe^{2+} ion toward Gly321, Fig 9(A). The distances from

488 C2 and C3 of the proximal ring to the water that marks the dioxygen binding site are 2.6 Å and 2.3 Å,

489 and the distances to Fe^{2+} are 4.5 Å and 4.1 Å. The best pose for BphAE$_{B356}$ is similar, Supplementary

490 Fig 4(A), but the C2 and C3 atoms are more distant from the water atom, 3.3 Å and 3.1 Å, and the Fe^{2+}

491 ion, 4.9 Å and 4.3 Å. The trichloromethyl group points in a similar direction toward Gly319 (aligns

492 with Gly321 of BphAE$_{II9}$).

493 In the best pose for the BphAE$_{LB400}$ complex, the C2 and C3 atoms lie 3.4 Å from the water and 4.0 Å

494 and 4.1 Å from the Fe^{2+}, however, the trichloromethyl group lies near Phe378 and the Fe^{2+} ion as

495 shown in Supplementary Fig 4(B) such that the shortest Cl-Fe^{2+} distance is 4.1 Å. Moreover, although

496 the C-water and C-Fe^{2+} distances are similar in the three docked complexes, the geometric relationships

497 between the ring, the water, and the Fe^{2+} in BphAE$_{LB400}$ differ markedly. In the BphAE$_{II9}$ and

498 BphAE$_{B356}$ complexes, the plane defined by C2, C3, and the Fe^{2+} is nearly orthogonal to the plane of

499 the ring, and the water is only ~0.8 Å out of the C2-C3-Fe^{2+} plane but more than 2.0Å out of the plane

500 of the ring. By contrast, in the BphAE$_{LB400}$ complex, the angle between the planes is ~45° and the

501 water is ~1.5 Å away from the the C2-C3-Fe^{2+} plane and within 1.0 Å of the plane of the ring.

502 Therefore, our study demonstrates that BphAE$_{II9}$ and BphAE$_{B356}$ have a similar level of activity

503 towards DDT. This finding is further supported by the docking study that shows BphAE$_{B356}$ and

504 BphAE$_{II9}$ have preferred binding poses for DDT that were quite similar. Unlike the other two enzymes,

505 BphAE$_{LB400}$ metabolized DDT very poorly and the docking experiments generated a binding pose that

506 was completely different from that of the other two enzymes. On the basis of biochemical data, the

507 preferred binding pose modeled in BphAE$_{LB400}$ is not a productive orientation. However, if DDT was

508 oriented in BphAE$_{LB400}$ in a way similar to what was observed in the docking with BphAE$_{II9}$, the

509 substrate would interfere with Gly321-Gln322 and Phe336. This interference is not present in

510 BphAE$_{II9}$ due to the substitution of Phe336 with Ile and the elimination of a hydrogen bond that

511 constrains the position of Gly321-Gln322.

512 In conclusion, our study of the structure of BphAE$_{II9}$ suggests an enzyme with increased flexibility in

513 and around its active site when compared to its two parent enzymes. This increased flexibility would

514 allow it to better accommodate a wide variety of potential substrates and this is reflected in its

515 enhanced substrate profile compared to its parent enzymes.

516

517 **Acknowledgement**

525

References

527   1.   **Cookson Jr, J. T.** 1995. Bioremediation engineering: design and application. McGraw-Hill, Inc.
528   2.   **Juhasz, A. L., and R. Naidu.** 2000. Bioremediation of high molecular weight polycyclic aromatic
529   hydrocarbons: a review of the microbial degradation of benzo-a-pyrene. International Biodeterioration &
530   Biodegradation **45:**57-88.
531   3.   **Safe, S. H.** 1994. Polychlorinated biphenyls (PCBs): environmental impact, biochemical and toxic
532   responses, and implications for risk assessment. CRC Critical Reviews in Toxicology **24:**87-149.
533   4.   **Safe, S.** 1990. Polychlorinated biphenyls (PCBs), dibenzo-p-dioxins (PCDDs), dibenzofurans (PCDFs),
534   and related compounds: environmental and mechanistic considerations which support the development
535   of toxic equivalency factors (TEFs). CRC Critical Reviews in Toxicology **21:**51-88.
536   5.   **Jacobson, J. L., S. W. Jacobson, and H. E. B. Humphrey.** 1990. Effects of in utero exposure to
537   polychlorinated biphenyls and related contaminants on cognitive functioning in young children. The
538   Journal of pediatrics **116:**38-45.
539   6.   **Van den Berg, M., L. Birnbaum, A. T. Bosveld, B. Brunström, P. Cook, M. Feeley, J. P. Giesy, A.**
540   **Hanberg, R. Hasegawa, and S. W. Kennedy.** 1998. Toxic equivalency factors (TEFs) for PCBs,
541   PCDDs, PCDFs for humans and wildlife. Environmental health perspectives **106:**775.
542   7.   **Patandin, S., C. I. Lanting, P. G. H. Mulder, E. R. Boersma, P. J. J. Sauer, and N. Weisglas-**
543   **Kuperus.** 1999. Effects of environmental exposure to polychlorinated biphenyls and dioxins on
544   cognitive abilities in Dutch children at 42 months of age. The Journal of pediatrics **134:**33-41.
545   8.   **Abraham, W.-R., B. Nogales, P. N. Golyshin, D. H. Pieper, and K. N. Timmis.** 2002.
546   Polychlorinated biphenyl-degrading microbial communities in soils and sediments. Current Opinion in
547   Microbiology **5:**246-253.
548   9.   **Unterman, R., D. L. Bedard, M. J. Brennan, L. H. Bopp, F. J. Mondello, R. E. Brooks, D. P.**
549   **Mobley, J. B. McDermott, C. C. Schwartz, and D. K. Dietrich.** 1988. Biological approaches for
550   polychlorinated biphenyl degradation. Basic Life Sci **45:**253-269.
551   10.   **Furukawa, K.** 1995. Presented at the Bioremediation: The Tokyo'94 Workshop,[27-30 November 1994].
552   11.   **Pieper, D. H.** 2005. Aerobic degradation of polychlorinated biphenyls. Applied microbiology and
553   biotechnology **67:**170-191.
554   12.   **Kumar, P., M. Mohammadi, J.-F. o. Viger, D. Barriault, L. Gomez-Gil, L. D. Eltis, J. T. Bolin, and**
555   **M. Sylvestre.** 2011. Structural insight into the expanded PCB-degrading abilities of a biphenyl
556   dioxygenase obtained by directed evolution. Journal of molecular biology **405:**531-547.
557   13.   **Colbert, C. L., N. Y. R. Agar, P. Kumar, M. N. Chakko, S. C. Sinha, J. B. Powlowski, L. D. Eltis,**
558   **and J. T. Bolin.** 2013. Structural characterization of Pandoraea pnomenusa B-356 biphenyl dioxygenase
559   reveals features of potent polychlorinated biphenyl-degrading enzymes. PloS one **8:**e52550.
560   14.   **Dhindwal, S., D. N. Patil, M. Mohammadi, M. Sylvestre, S. Tomar, and P. Kumar.** 2011.
561   Biochemical studies and ligand-bound structures of biphenyl dehydrogenase from Pandoraea pnomenusa
562   strain B-356 reveal a basis for broad specificity of the enzyme. Journal of Biological Chemistry
563   **286:**37011-37022.

564   15.   **Hülsmeyer, M., H.-J. Hecht, K. Niefind, D. Schomburg, B. Hofer, K. N. Timmis, and L. D. Eltis.**
565   1998. Crystal structure of cis-biphenyl-2,3-dihydrodiol-2,3-dehydrogenase from a PCB degrader at 2.0
566   Å resolution. Protein Science **7:**1286-1293.
567   16.   **Sato, N., Y. Uragami, T. Nishizaki, Y. Takahashi, G. Sazaki, K. Sugimoto, T. Nonaka, E. Masai,**
568   **M. Fukuda, and T. Senda.** 2002. Crystal structures of the reaction intermediate and its homologue of
569   an extradiol-cleaving catecholic dioxygenase. Journal of molecular biology **321:**621-636.
570   17.   **Horsman, G. P., J. Ke, S. Dai, S. Y. K. Seah, J. T. Bolin, and L. D. Eltis.** 2006. Kinetic and structural
571   insight into the mechanism of BphD, a CC bond hydrolase from the biphenyl degradation pathway.
572   Biochemistry **45:**11071-11086.
573   18.   **Erickson, B. D., and F. J. Mondello.** 1992. Nucleotide sequencing and transcriptional mapping of the
574   genes encoding biphenyl dioxygenase, a multicomponent polychlorinated-biphenyl-degrading enzyme in
575   Pseudomonas strain LB400. Journal of bacteriology **174:**2903-2912.
576   19.   **Fain, M. G., and J. D. Haddock.** 2001. Phenotypic and phylogenetic characterization of Burkholderia
577   (Pseudomonas) sp. strain LB400. Current microbiology **42:**269-275.
578   20.   **Furusawa, Y., V. Nagarajan, M. Tanokura, E. Masai, M. Fukuda, and T. Senda.** 2004. Crystal
579   Structure of the Terminal Oxygenase Component of Biphenyl Dioxygenase Derived from *Rhodococcus*
580   sp. Strain RHA1. Journal of molecular biology **342:**1041-1052.
581   21.   **Parales, R. E., J. V. Parales, and D. T. Gibson.** 1999. Aspartate 205 in the catalytic domain of
582   naphthalene dioxygenase is essential for activity. Journal of bacteriology **181:**1831-1837.
583   22.   **Brühlmann, F., and W. Chen.** 1999. Tuning biphenyl dioxygenase for extended substrate specificity.
584   Biotechnology and bioengineering **63:**544-551.
585   23.   **Kumamaru, T., H. Suenaga, M. Mitsuoka, T. Watanabe, and K. Furukawa.** 1998. Enhanced
586   degradation of polychlorinated biphenyls by directed evolution of biphenyl dioxygenase. Nature
587   biotechnology **16:**663-666.
588   24.   **Mondello, F. J., M. P. Turcich, J. H. Lobos, and B. D. Erickson.** 1997. Identification and
589   modification of biphenyl dioxygenase sequences that determine the specificity of polychlorinated
590   biphenyl degradation. Applied and environmental microbiology **63:**3096-3103.
591   25.   **Barriault, D., M.-M. l. Plante, and M. Sylvestre.** 2002. Family shuffling of a targeted bphA region to
592   engineer biphenyl dioxygenase. Journal of bacteriology **184:**3794-3800.
593   26.   **Barriault, D., and M. Sylvestre.** 2004. Evolution of the biphenyl dioxygenase BphA from Burkholderia
594   xenovorans LB400 by random mutagenesis of multiple sites in region III. Journal of Biological
595   Chemistry **279:**47480-47488.
596   27.   **Mohammadi, M., J. F. Viger, P. Kumar, D. Barriault, J. T. Bolin, and M. Sylvestre.** 2011. Retuning
597   Rieske-type oxygenases to expand substrate range. Journal of Biological Chemistry **286:**27612-27621.
598   28.   **Kumar, P., M. Mohammadi, S. Dhindwal, T. T. M. Pham, J. T. Bolin, and M. Sylvestre.** 2012.
599   Structural insights into the metabolism of 2-chlorodibenzofuran by an evolved biphenyl dioxygenase.
600   Biochemical and biophysical research communications **421:**757-762.
601   29.   **Gómez-Gil, L., P. Kumar, D. Barriault, J. T. Bolin, M. Sylvestre, and L. D. Eltis.** 2007.
602   Characterization of biphenyl dioxygenase of Pandoraea pnomenusa B-356 as a potent polychlorinated
603   biphenyl-degrading enzyme. Journal of bacteriology **189:**5705-5715.
604   30.   **Vagin, A., and A. Teplyakov.** 1997. MOLREP: an automated program for molecular replacement.
605   Journal of Applied Crystallography **30:**1022-1025.
606   31.   **Bailey, S.** 1993. The CCP4 suite: programs for protein crystallography. Daresbury Laboratory.
607   32.   **Murshudov, G. N., A. A. Vagin, and E. J. Dodson.** 1997. Refinement of macromolecular structures by
608   the maximum-likelihood method. Acta Crystallographica Section D: Biological Crystallography **53:**240-
609   255.
610   33.   **Emsley, P., and K. Cowtan.** 2004. Coot: model-building tools for molecular graphics. Acta
611   Crystallographica Section D: Biological Crystallography **60:**2126-2132.

612   34.   **Davis, I. W., A. Leaver-Fay, V. B. Chen, J. N. Block, G. J. Kapral, X. Wang, L. W. Murray, W. B.**
613   **Arendall, J. Snoeyink, and J. S. Richardson.** 2007. MolProbity: all-atom contacts and structure
614   validation for proteins and nucleic acids. Nucleic acids research **35:**W375-W383.
615   35.   **DeLano, W. L.** 2002. The PyMOL molecular graphics system.
616   36.   **Hurtubise, Y., D. Barriault, and M. Sylvestre.** 1996. Characterization of active recombinant his-
617   tagged oxygenase component of Comamonas testosteroni B-356 biphenyl dioxygenase. Journal of
618   Biological Chemistry **271:**8152-8156.
619   37.   **Pham, T. T. M., and M. Sylvestre.** 2013. Has the bacterial biphenyl catabolic pathway evolved
620   primarily to degrade biphenyl? The diphenylmethane case. Journal of bacteriology **195:**3563-3574.
621   38.   **L'Abbée, J.-B., Y. Tu, D. Barriault, and M. Sylvestre.** 2011. Insight into the metabolism of 1, 1, 1-
622   trichloro-2, 2-bis (4-chlorophenyl) ethane (DDT) by biphenyl dioxygenases. Archives of Biochemistry
623   and Biophysics **516:**35-44.
624   39.   **Schrodinger, L. L. C.** 2009. Maestro. Schrodinger LLC, New York.
625   40.   **Friesner, R. A., J. L. Banks, R. B. Murphy, T. A. Halgren, J. J. Klicic, D. T. Mainz, M. P.**
626   **Repasky, E. H. Knoll, M. Shelley, and J. K. Perry.** 2004. Glide: a new approach for rapid, accurate
627   docking and scoring. 1. Method and assessment of docking accuracy. Journal of medicinal chemistry
628   **47:**1739-1749.
629   41.   **Halgren, T. A., R. B. Murphy, R. A. Friesner, H. S. Beard, L. L. Frye, W. T. Pollard, and J. L.**
630   **Banks.** 2004. Glide: a new approach for rapid, accurate docking and scoring. 2. Enrichment factors in
631   database screening. Journal of medicinal chemistry **47:**1750-1759.
632   42.   **Karlsson, A., J. V. Parales, R. E. Parales, D. T. Gibson, H. Eklund, and S. Ramaswamy.** 2003.
633   Crystal structure of naphthalene dioxygenase: side-on binding of dioxygen to iron. Science **299:**1039-
634   1042.
635   43.   **Seeger, M., M. Zielinski, K. N. Timmis, and B. Hofer.** 1999. Regiospecificity of dioxygenation of di-
636   to pentachlorobiphenyls and their degradation to chlorobenzoates by the bph-encoded catabolic pathway
637   of Burkholderia sp. strain LB400. Applied and environmental microbiology **65:**3614-3621.
638   44.   **Haddock, J. D., J. R. Horton, and D. T. Gibson.** 1995. Dihydroxylation and dechlorination of
639   chlorinated biphenyls by purified biphenyl 2, 3-dioxygenase from Pseudomonas sp. strain LB400.
640   Journal of bacteriology **177:**20-26.
641   45.   **Suenaga, H., M. Mitsuoka, Y. Ura, T. Watanabe, and K. Furukawa.** 2001. Directed evolution of
642   biphenyl dioxygenase: emergence of enhanced degradation capacity for benzene, toluene, and
643   alkylbenzenes. Journal of bacteriology **183:**5441-5444.
644   46.   **Suenaga, H., A. Nishi, T. Watanabe, M. Sakai, and K. Furukawa.** 1999. Engineering a hybrid
645   pseudomonad to acquire 3, 4-dioxygenase activity for polychlorinated biphenyls. Journal of bioscience
646   and bioengineering **87:**430-435.
647   47.   **Kimura, N., A. Nishi, M. Goto, and K. Furukawa.** 1997. Functional analyses of a variety of chimeric
648   dioxygenases constructed from two biphenyl dioxygenases that are similar structurally but different
649   functionally. Journal of bacteriology **179:**3936-3943.
650

651   **Figure legend:**

652   **Fig 1:** A) Schematic representation of the first enzyme of biphenyl catabolic pathway exhibiting its

653   three components. B) Displaying the bound biphenyl in BphAE$_{II9}$ with Fo - Fc electron density

654   contoured at 3σ. Residues surrounding the biphenyl are shown in stick models. The Fe^{2+} atom and

655   water molecule are shown as spheres.

656   **Fig 2:** Superposition of all the chains of A) $BphAE_{LB400}$ biphenyl bound, B) $BphAE_{II9}$ biphenyl bound

657   C) $BphAE_{II9}$ substrate free structure with Fe^{2+} and conserved water atom has been shown exhibiting the

658   differences in the conformation of the residues at the active site. For distinction, five Fe^{2+} ions in

659   cluster I (chains A, C, E, G and U) are colored orange and in cluster II (chains I, K, M, O, Q and W)

660   are colored blue. In chain S, Fe^{2+} is colored yellow. Water molecules bound at the active site are

661   colored red. The red box accentuates the alterations in Asp388 residue in $BphAE_{II9}$ biphenyl bound

662   structure in comparison with other structures.

663   **Fig 3:** Stereo view showing the active site region of $BphAE_{LB400}$ (blue), $BphAE_{B356}$ (red), $BphAE_{II9}$-

664   biphenyl bound (green), $BphAE_{II9}$-biphenyl free (magenta) superposed over each other. (A) The

665   variation in the position of carbonyl towards the active site in $BphAE_{LB400}$, in $BphAE_{II9}$-biphenyl free

666   structure and away from the active site in $BphAE_{II9}$ due to mutation in residue Thr335Gly has been

667   shown. (B) The effect of residue Thr at position 335 in $BphAE_{LB400}$ and the effect of its mutation to

668   Gly in $BphAE_{II9}$ has been shown. B) The effect of residue Phe at position 336 in $BphAE_{LB400}$ and the

669   effect of its mutation to Ile in $BphAE_{II9}$ has been shown. C) The effect of residue Asn at position 338

670   in $BphAE_{LB400}$ and the effect of its mutation to Thr in $BphAE_{II9}$ has been shown. For ease, Fe^{2+} has

671   been colored with the corresponding color of carbon in each structure. The dotted line in yellow has

672   been used to show the distances measured in Å. The other dotted lines in blue, red and green highlights

673   hydrogen bond in $BphAE_{LB400}$, $BphAE_{B356}$ and $BphAE_{II9}$-biphenyl bound with surrounding residues

674   respectively.

675 **Fig 4:** Figure showing the overall differences at the active site of $BphAE_{II9}$ (in cyan color) due to

676 mutation in comparison with the ligand bound state of $BphAE_{LB400}$ (in green color). The red arrows

677 show the effect of residues at position 336, 338, and Arg340 on Phe378. The boxes in red color show

678 other important regions where large differences have been found between $BphAE_{LB400}$ and $BphAE_{B356}$.

679 For ease, the Fe^{2+} ion has been colored with the corresponding color of carbon in each structure. The

680 dotted line in yellow has been used to show the distances measured in Å.

681 **Fig 5:** Total ion chromatogram showing A) the peak of the metabolite produced from 2,3,4'-

682 trichlorobiphenyl and the peak of the substrate remaining after 15 min reaction by reconstituted His-

683 tagged $BphAE_{II9}$ (black curve), $BphAE_{LB400}$ (gray curve), B) the peak of the metabolite produced from

684 2,2',5,5'-tetrachlorobiphenyl and the peak of the substrate remaining after 15 min reaction by

685 reconstituted His-tagged $BphAE_{II9}$ (black curve), $BphAE_{LB400}$ (gray curve), C) the peaks of the two

686 stereoisomer metabolites produced from DDT after 15 min reaction by reconstituted His-tagged

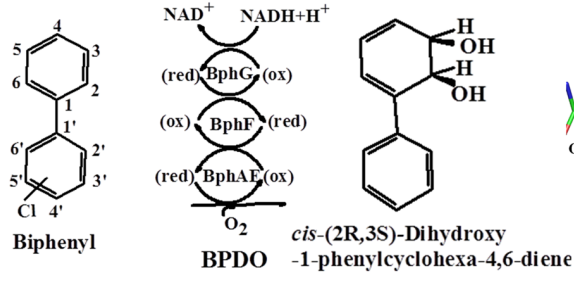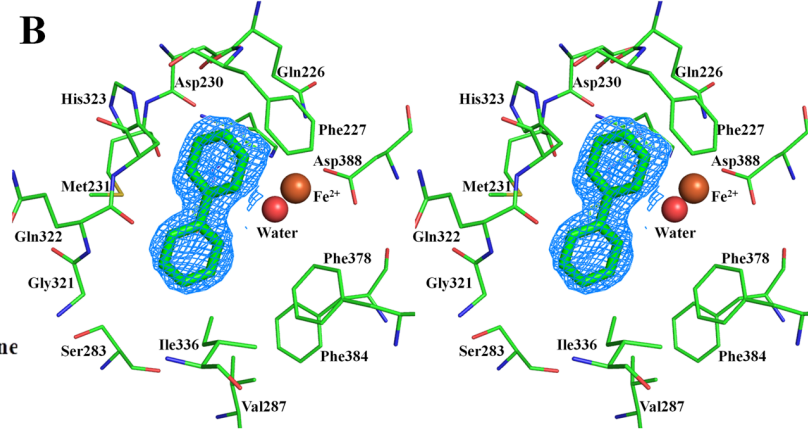687 $BphAE_{II9}$ (grey curve), $BphAE_{B356}$(black curve).

688 **Fig 6:** Stereo view of structure of (A) $BphAE_{II9}$ & (B) superposed structures of $BphAE_{LB400}$ (red),

689 $BphAE_{B356}$ (blue), and $BphAE_{II9}$ (yellow-orange) at the active site in the presence of Fe^{2+} and water

690 molecule with the surrounding residues with docked 2,3,4'-trichlorobiphenyl in a pose which has

691 shown maximum biochemical output, *i.e*, 4,5-dioxygenation. The color mentioned above corresponds

692 to the color of carbon in the figure. Chlorine atoms are green, oxygen atoms are red, and nitrogen

693 atoms are blue. For ease, the Fe^{2+} ion and water have been colored with the corresponding color of

694 carbon in each structure. The sphere with the larger radius corresponds to Fe^{2+} and the other to the

695 water. The dashed lines are the calculated distances measured in Å from docked substrate and Fe^{2+} or
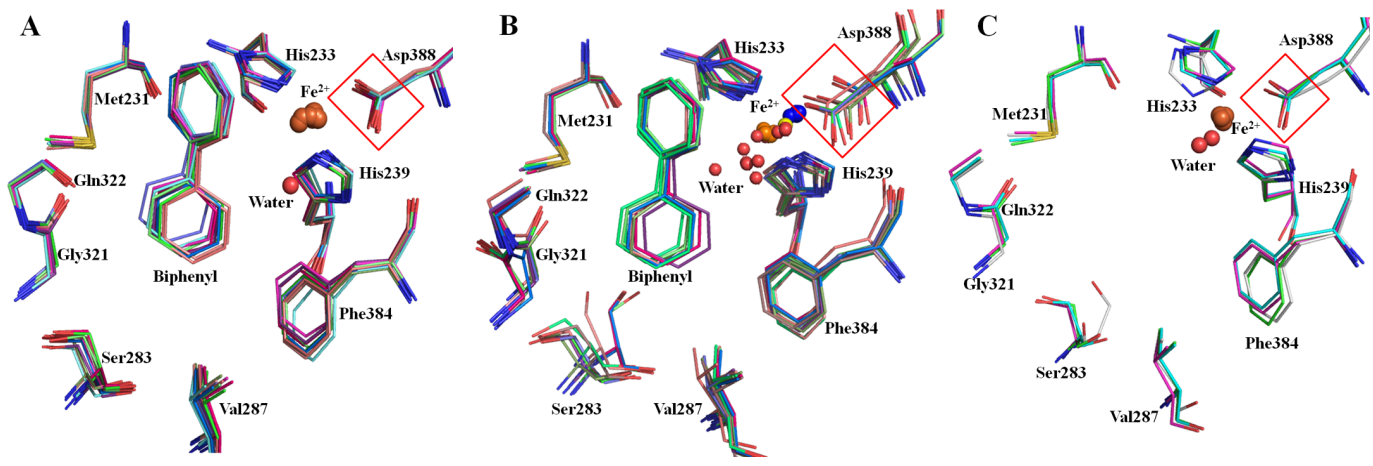
696 water molecule.

697   **Fig 7:** Stereo view of structure of (A) $BphAE_{II9}$ & (B) superposed structures of $BphAE_{LB400}$ (red),

698    $BphAE_{B356}$ (blue), and $BphAE_{II9}$ (yellow-orange) at the active site in the presence of Fe^{2+} and water

699   molecule with the surrounding residues with docked 2,5,2',5'-tetrachlorobiphenyl in a pose which has

700   shown maximum biochemical output, *i.e*, 3,4-dioxygenation. The color mentioned above corresponds

701   to the color of carbon in the figure. Chlorine atoms are green, oxygen atoms are red, and nitrogen

702   atoms are blue. For ease, the Fe^{2+} ion and water have been colored with the corresponding color of

703   carbon in each structure. The sphere with the larger radius corresponds to Fe^{2+} and the other to the

704   water. The dashed lines are the calculated distances measured in Å from docked substrate and Fe^{2+} or
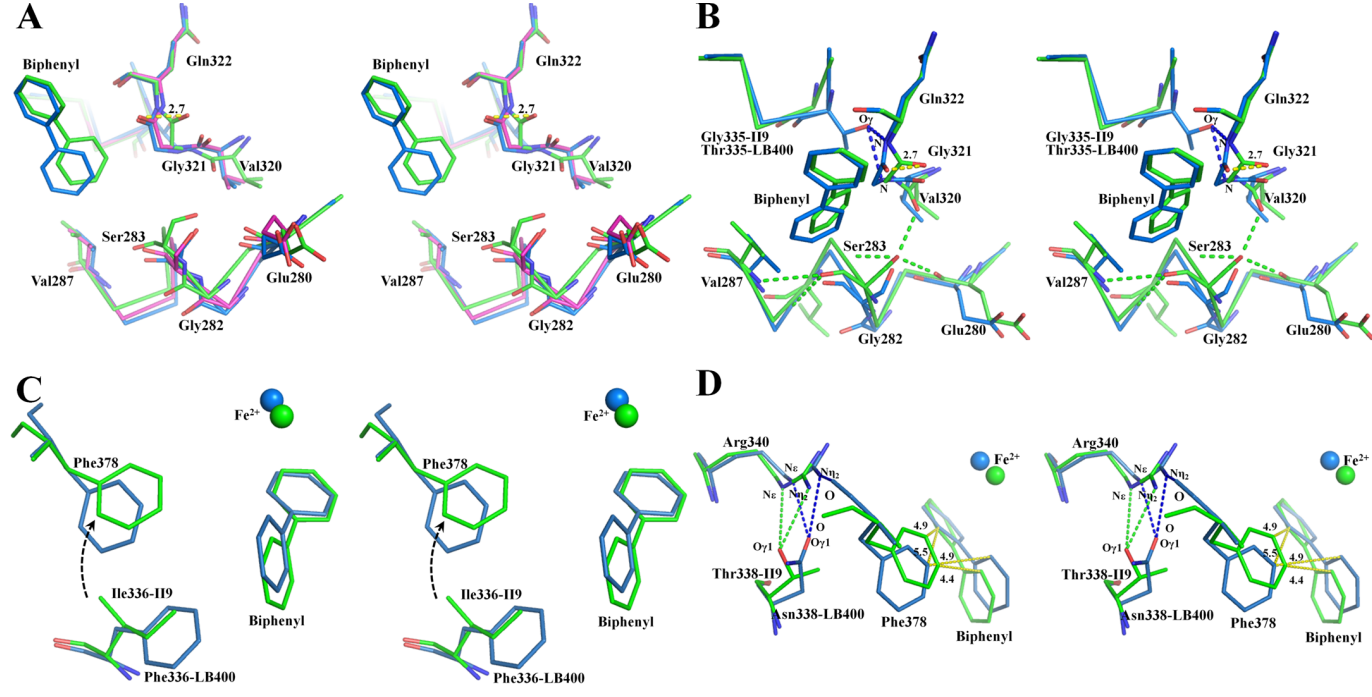
705   water molecule.

706   **Fig 8:** Stereo view of structure of (A) $BphAE_{II9}$ & (B) superposed structures of $BphAE_{LB400}$ (red),

707    $BphAE_{B356}$ (blue), and $BphAE_{II9}$ (yellow-orange) at the active site in the presence of Fe^{2+} and water

708   molecule with the surrounding residues with docked 2,5,2',5'-tetrachlorobiphenyl showing the effect of

709   Thr375 in $BphAE_{B356}$ and corresponding residue Asn377 in $BphAE_{LB400}$/$BphAE_{II9}$ is shown. For ease,

710   the Fe^{2+} ion and water have been colored with the corresponding color of carbon in each structure. The

711   sphere with the larger radius corresponds to Fe^{2+} and the other to the water. The blue, red and yellow-

712   orange dotted line shows the H-bond interactions of different residues in $BphAE_{B356}$, $BphAE_{LB400}$ and
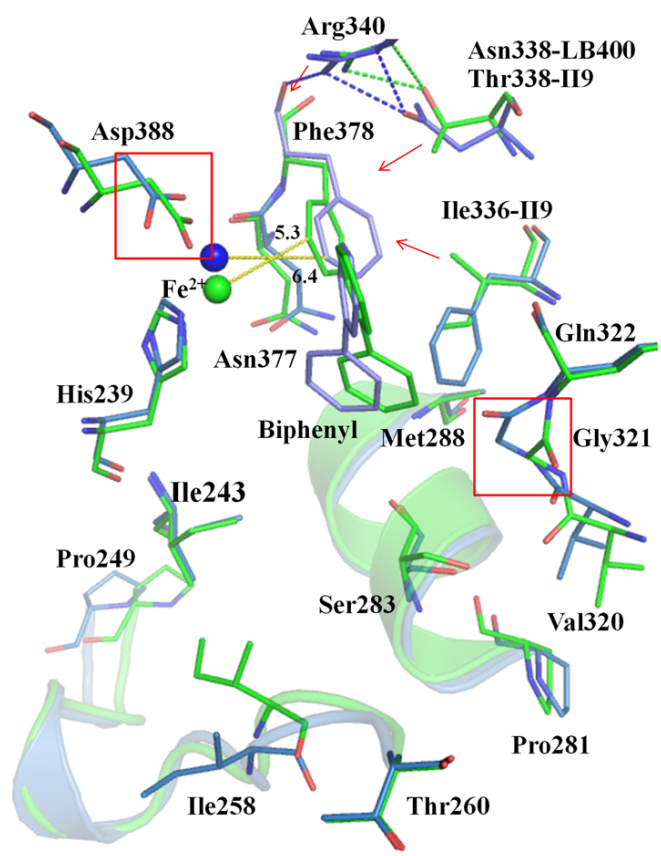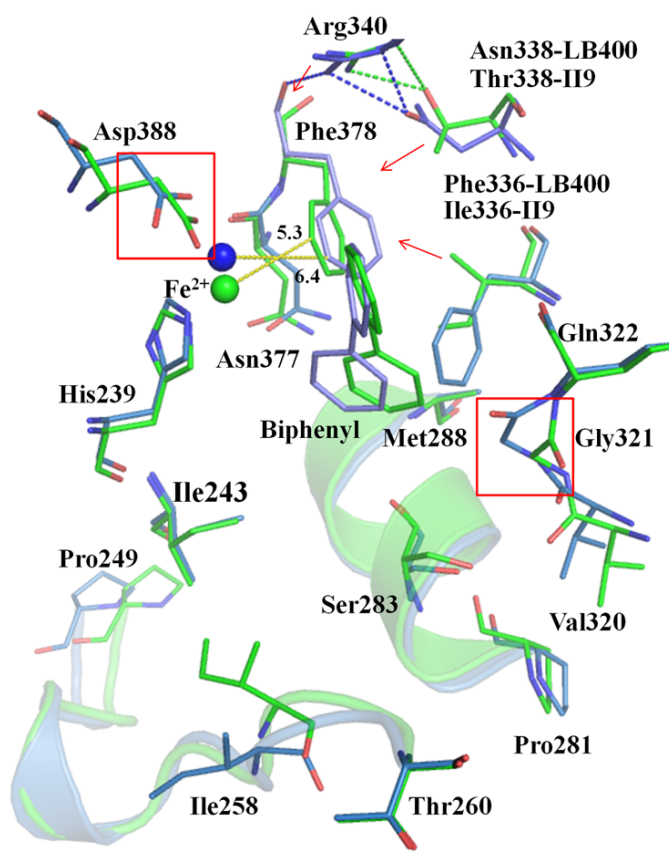
713    $BphAE_{II9}$.

714   **Fig 9:** Stereo view of structure of (A) $BphAE_{II9}$ & (B) superposed structures of $BphAE_{LB400}$ (red),

715    $BphAE_{B356}$ (blue), and $BphAE_{II9}$ (yellow-orange) at the active site in the presence of Fe^{2+} and water

716   molecule with the surrounding residues with docked DDT in a pose which has shown maximum

717   biochemical output, *i.e*, 2,3-dioxygenation. The color mentioned above corresponds to the color of

718   carbon in the figure. Chlorine atoms are green, oxygen atoms are red, and nitrogen atoms are blue. For

719   ease, the Fe^{2+} ion and water have been colored with the corresponding color of carbon in each
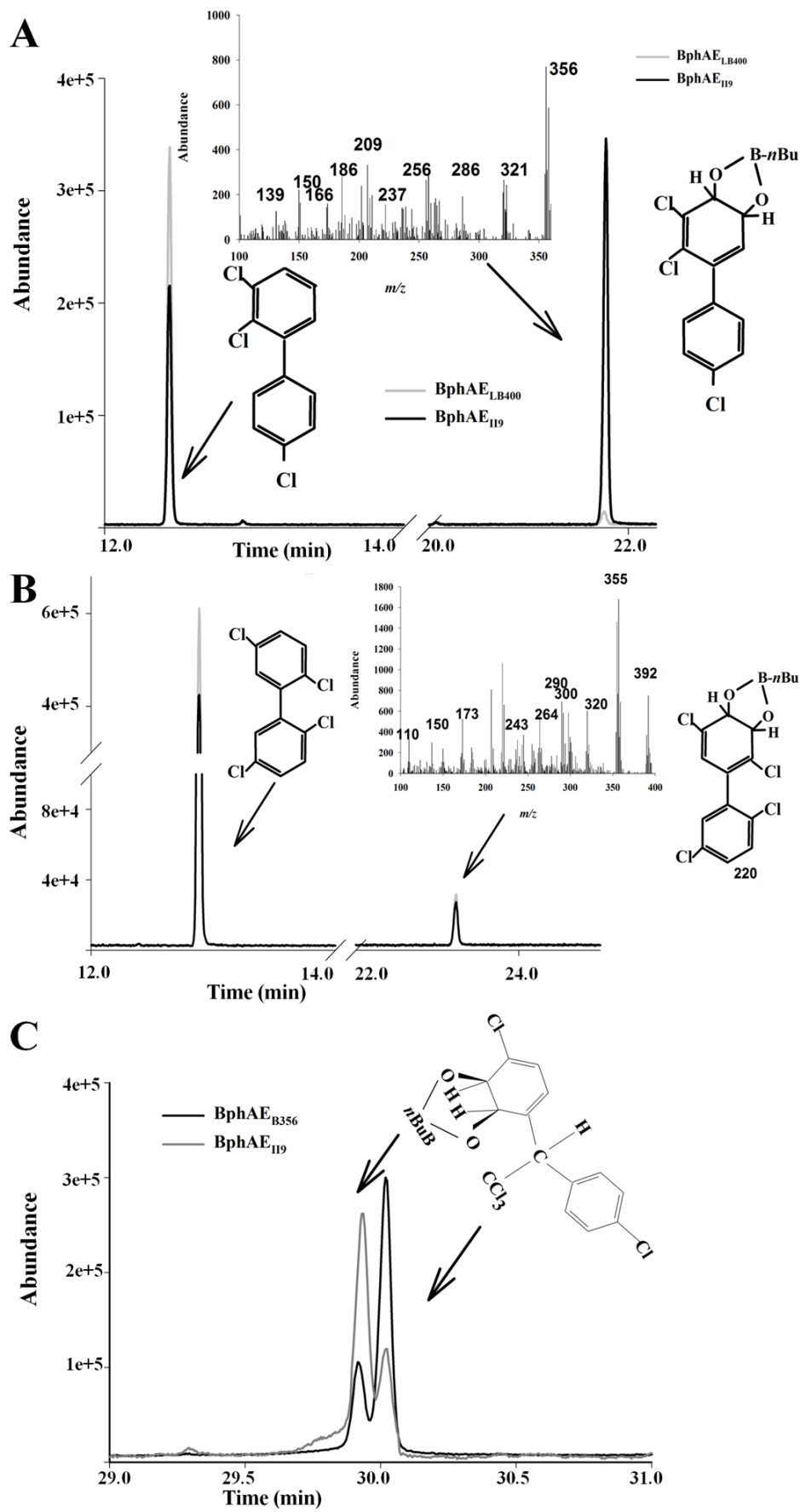
720   structure. The sphere with the larger radius corresponds to Fe^{2+} and the other to the water. The dashed

721   lines are the calculated distances measured in Å from docked substrate and Fe^{2+} or water molecule.

A

Biphenyl

BPDO

cis-(2R,3S)-Dihydroxy -1-phenylcyclohexa-4,6-diene

B

A

Biphenyl
Gln322
2.7
Gly321 Val320
Ser283
Val287
Gly282
Glu280

B

Gly335-II9
Thr335-LB400
Biphenyl
Oγ
Gln322
2.7 Gly321
N Val320
Ser283
Val287
Gly282 Glu280

C

Fe²⁺
Phe378
Ile336-II9
Phe336-LB400
Biphenyl

D

Arg340
Nε Nη2
Nε
Oγ1 Oγ1
O
Thr338-II9
Asn338-LB400
Phe378
5.5 4.9
4.9
4.4
Biphenyl
Fe²⁺

A

Ile336

Phe378

Gln322

Gly321

2,3,4'-trichloro biphenyl

3 4 3.3

2 3.0

5 5.1

4.5

HOH

Fe²⁺

4'

Pro259

Ile258

Ile243

B

Ile336/
Phe-LB400

Phe378

Gln 322

Gly 321

2,3,4'-trichloro biphenyl

HOH

Fe²⁺

Pro259

Ile258

Ile243

A

Fe²⁺
HOH
Phe378
Ile336
His239
Gln 322
Gly321
2,5,2',5'-tetra chloro biphenyl
Ser283
Ile258
Pro259

B

Fe²⁺
HOH
Phe378
Ile336/
Phe-LB400
His239
Gln 322
Gly321
2,5,2',5'-tetra chloro biphenyl
Ser283
Ile258
Pro259

His373-LB400/II9   Val287   2,5,2',5'-tetrachloro biphenyl

Gln371-B356

Asn377-LB400/II9
Thr375-B356

Phe378/376

HOH

Fe^{2+}

His373-LB400/II9   Val287   2,5,2',5'-tetrachloro biphenyl

Gln371-B356

Asn377-LB400/II9
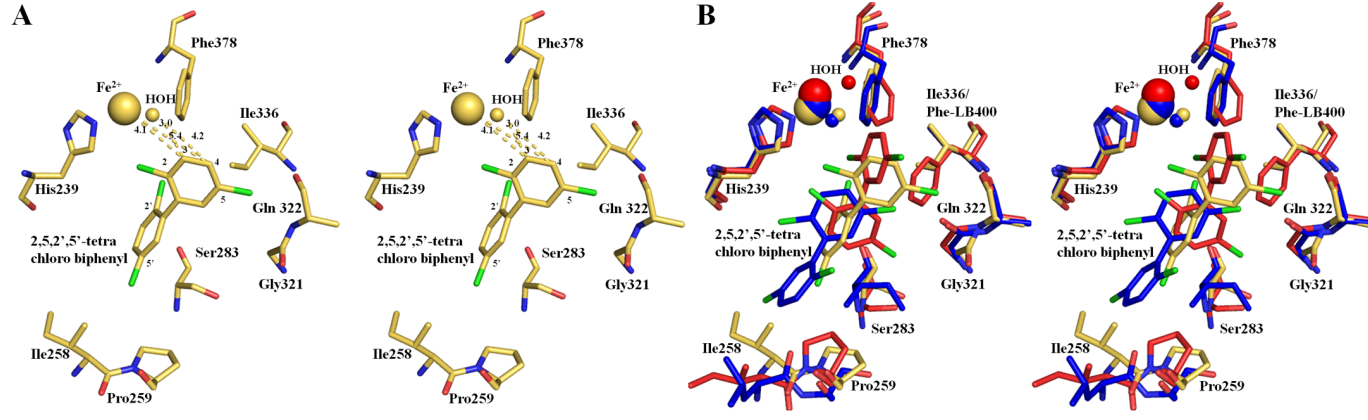Thr375-B356
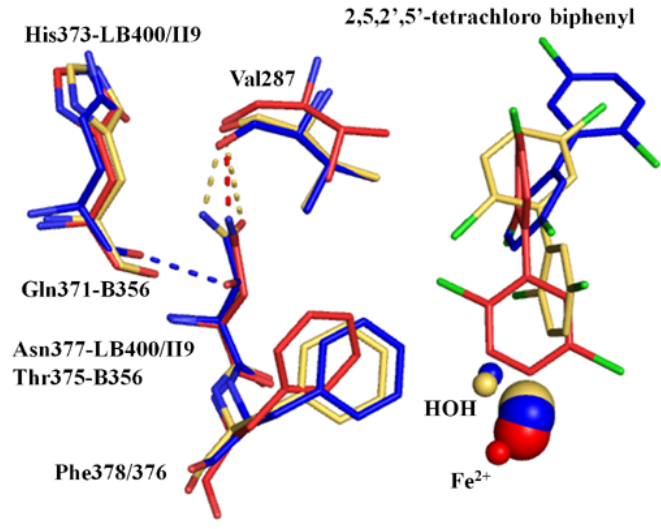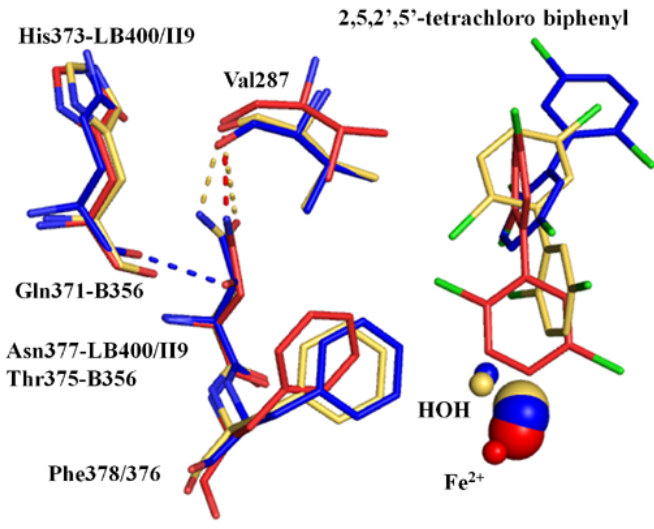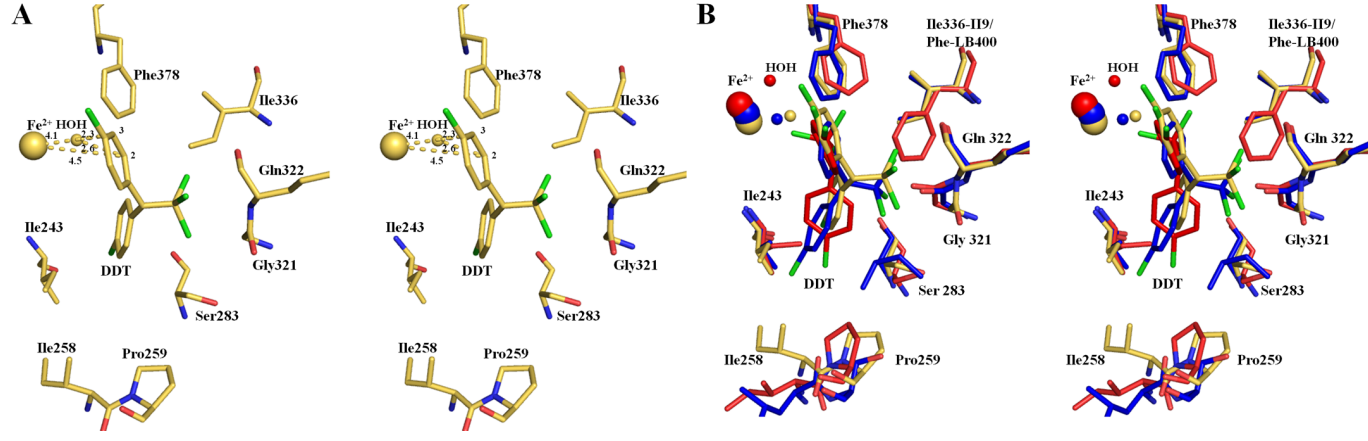
Phe378/376

HOH

Fe^{2+}

A

B

Table Title:

Table1: Data collection and refinement statistics for biphenyl-free and biphenyl-bound structure of BphAE$_{II9}$.

	BphAE$_{II9}$ biphenyl-free (PDB ID: 5AEU)	BphAE$_{II9}$ biphenyl- bound (PDB ID: 5AEW)
Crystallographic data		
Space group	*H3*	*P1*
Wavelength (Å)	0.9	0.9
Resolution	129.1 - 2.5	129.1 - 1.9
Cell dimensions		
a (Å)	211.89	132.77
b (Å)	211.89	133.19
c (Å)	168.44	133.96
α (°)	90	102.31
β (°)	90	102.54
γ (°)	120	104.54
Unique reflections	97519	634861
Completeness (%) (Last shell)	99.4 (99.9)	94.0 (92.0)
R_{sym}(%)[a] (Last Shell)	10.0 (53.0)	10.0 (40.0)
I/σ (Last shell)	9.3 (2.6)	21 (3.3)
V_M (Å^3 Da^{-1})	2.3 (46 % solvent)	2.3 (46 % solvent)
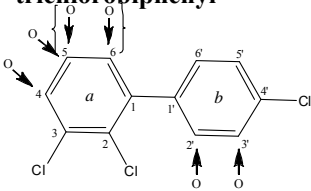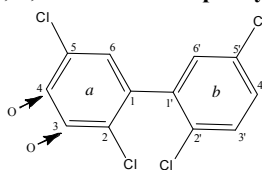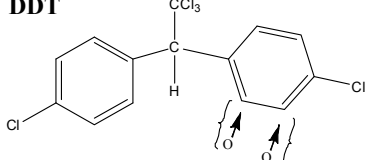
Refinement		
No. of reflections (working/test)	92654/4632	618963/30948
No. of residues	2463	7368
Water molecules	389	4008
Resolution range (Å)	38.6 - 2.5	23.3 - 1.9
R_{work} (%)	18.1	21.6
R_{free} (%)	23.4	25.4
Average B-factors (Å^2)		
Protein chains	AB 33.9	AB 33.9
	CD 40.1	CD 40.1
	EF 49.3	EF 49.3
	GH 51.8	GH 51.8
		IJ 16.4
		KL 21.0
		MN 23.4
		OP 18.6
		QR 23.2
		ST 28.7
		UV 30.1
		WX 34.2
Water Atoms	44.0	36.4
All atoms	44.0	24.3
r.m.s.d on bond lengths (Å)	0.008	0.005

r.m.s.d on bond angles (Å)	1.25	1.07
Ramachandran plot (%)		
Favored	98.0	96.3
Allowed	99.8	99.9
Outliers (no. of residues)	4	11

a

$$R_{sym} = \sum_{hkl} \sum_{i=1}^{n} \left| I_{hkl,i} - \overline{I}_{hkl} \right| \Big/ \sum_{hkl} \sum_{i=1}^{n} I_{hkl,i}$$

Table 2: Table showing the probable sites for dioxygenation, the distances from those carbons to water and Fe^{2+}, the Glide score, and the Emodel value for the docking of 2,3,4'-trichlorobiphenyl, 2,2',5,5'-tetrachlorobiphenyl and DDT at the active site of BphAE$_{LB400}$, BphAE$_{B356}$, and BphAE$_{II9}$.

PCB	BPDO Variant	Position for dioxygenation		Distance (Å) from		Glide score	Emodel
				Water	Fe^{2+}		
2,3,4'-trichlorobiphenyl	II9	4,5	*m,p*	3.3	5.1	-6.48	-37.24
				3.0	4.5		
	LB400	4,5	*m,p*	2.8	4.3	-7.13	-39.21
				3.0	4.4		
	B356	4,5	*m,p*	3.4	5.1	-5.30	-21.19
				3.1	4.8		
2,5,2',5'-tetrachlorobiphenyl	II9	3,4	*m,p*	3.0	4.1	-5.43	-11.47
				4.2	5.4		
	LB400	3,4	*m,p*	3.3	4.2	-6.14	-27.950
				3.4	4.3		
	B356	3,4	*m,p*	4.1	5.6	-5.83	-37.81
				4.3	5.6		
DDT	II9	2,3	*o,m*	2.3	4.1	-7.61	-56.00
				2.6	4.5		
	B356	2,3	*o,m*	3.1	4.3	-6.01	-41.43

			3.3	4.9		
LB400	2,3	*o,m*	3.3	4.0	-5.61	-28.81
			3.4	4.1		